

Long-Range, Deep-Ocean Propagation of 15-Hz CW Acoustic Signals

R. FITZGERALD, J. D. SHAFFER, A. N. GUTHRIE,
D. A. NUTILE, AND W. R. HAHN

*Applied Ocean Acoustics Branch
Acoustics Division*

August 9, 1979



NAVAL RESEARCH LABORATORY
Washington, D.C.

Approved for public release; distribution unlimited.

SECURITY CLASSIFICATION OF THIS PAGE (When Data Entered)

REPORT DOCUMENTATION PAGE		READ INSTRUCTIONS BEFORE COMPLETING FORM
1. REPORT NUMBER NRL Report 8302	2. GOVT ACCESSION NO.	3. RECIPIENT'S CATALOG NUMBER
4. TITLE (and Subtitle) LONG-RANGE, DEEP-OCEAN PROPAGATION OF 15-Hz CW ACOUSTIC SIGNALS	5. TYPE OF REPORT & PERIOD COVERED Interim report on a continuing NRL problem	
	6. PERFORMING ORG. REPORT NUMBER	
7. AUTHOR(s) R. Fitzgerald, J.D. Shaffer, A.N. Guthrie, D.A. Nutile, and W.R. Hahn	8. CONTRACT OR GRANT NUMBER(s)	
9. PERFORMING ORGANIZATION NAME AND ADDRESS Naval Research Laboratory Washington, D.C. 20375	10. PROGRAM ELEMENT, PROJECT, TASK AREA & WORK UNIT NUMBERS NRL Problem S01-64.703 62759N; ZF52-552-003	
11. CONTROLLING OFFICE NAME AND ADDRESS Chief of Naval Material Navy Department Washington, D.C. 20360	12. REPORT DATE August 9, 1979	
	13. NUMBER OF PAGES 21	
14. MONITORING AGENCY NAME & ADDRESS (if different from Controlling Office)	15. SECURITY CLASS. (of this report) UNCLASSIFIED	
	15a. DECLASSIFICATION/DOWNGRADING SCHEDULE	
16. DISTRIBUTION STATEMENT (of this Report) Approved for public release; distribution unlimited.		
17. DISTRIBUTION STATEMENT (of the abstract entered in Block 20, if different from Report)		
18. SUPPLEMENTARY NOTES		
19. KEY WORDS (Continue on reverse side if necessary and identify by block number) Acoustic propagation Long range Low frequency		
20. ABSTRACT (Continue on reverse side if necessary and identify by block number) The acoustic field of a shallow continuous-wave source operating near 15 Hz was measured at a deep sound-channel hydrophone located near Midway Island. The source was towed repeatedly between 700-km range and 1700-km range along a great circle track whose extension passed through the receiver. Although the possibility of long-range transmission of low-frequency acoustic energy via bottom-bounce and bottom-penetrating paths has been postulated, analysis of the 15-Hz transmission loss curves indicates that the only long-range propagation paths of significance were those which did not interact with the bottom.		

DD FORM 1473
1 JAN 73EDITION OF 1 NOV 65 IS OBSOLETE
S/N 0102-014-6601

i

SECURITY CLASSIFICATION OF THIS PAGE (When Data Entered)

CONTENTS

DESCRIPTION OF THE EXPERIMENT	1
ENVIRONMENTAL DATA	2
Navigation	2
Bathymetry	2
Thermal Structure of the Water and Sound Speed Profiles ...	2
ACOUSTIC DATA	2
ACKNOWLEDGMENTS	19
REFERENCES	19

LONG-RANGE, DEEP-OCEAN PROPAGATION OF 15-Hz CW ACOUSTIC SIGNALS

DESCRIPTION OF THE EXPERIMENT

A ship towed two continuous-wave (CW) sources operating near 15 Hz at 140-m depth and 114 Hz at 21-m depth, dropped explosive charges on a regular schedule, and made environmental measurements. The acoustic signals were received on an omnidirectional sound-channel hydrophone which is suspended up from the bottom in deep water near Midway Island. The exercise lasted 14 days and was divided into five phases. During the exercise the ship made 47 expendable bathythermograph (XBT) casts and kept a continuous bathymetric record by using a precision fathometer (PFR).

Figure 1 is an abstract of the experimental geometry. The first phase was a great circle transit from the hydrophone area to a range of 700 km made to determine the environmental parameters along this track. Throughout the remaining phases, the acoustic sources were operated and the ship attempted to maintain a constant 7-knot speed. In the second phase, the ship continued along the extension of the great circle track of phase one to a range of 1700 km. In the third phase the ship reversed course and returned to a range of 700 km. The fourth phase repeated the second phase. The intention in the fifth phase was to have the ship steam in the direction transverse to the line of acoustic propagation. In fact, the ship proceeded roughly along a 600-km-long straight line track from the terminus of phase four at a 1650-km range to a point 1550 km from the hydrophone.

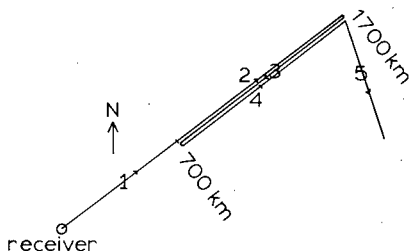


Fig. 1 — Abstract of the ship's track labeled to show the five phases of the experiment and the nominal range from the receiver at the beginning of each phase

The CW sources were controlled by a crystal standard. At the receiver, each CW signal was band-pass filtered, heterodyned to low frequency, low-pass filtered, and sampled once every two seconds. Signals from the explosives were analog recorded.

A description and a listing of the environmental data acquired have been published [1], as have the results from the shallow-explosive signals [2,3]. The 15-Hz CW signals from phase five have been analyzed and interpreted in terms of signal coherence along a line transverse to the direction of propagation [4]. This paper reports the 15-Hz CW transmission loss data obtained in phase two, three, and four.

ENVIRONMENTAL DATA

Navigation

The basic navigation data consisted of Navy Navigation Satellite System fixes as available plus Loran C fixes every 15 min. Some information about ship's speed was used to improve the navigation. We are confident that the ship's range is accurate continuously to ± 1 km during phases two, three, and four which are the subject of this paper. This accuracy is confirmed by the range-sensitive analysis [2] performed on the explosive signals. Figure 2 shows details of the navigation for phases two, three, and four.

Bathymetry

The bathymetry determined from the PFR records for an assumed sound speed of 1500 m/s is plotted in Fig. 3. Although not shown in this figure, the bottom rises in the vicinity of the hydrophone to a depth of about 3000 m. A brief survey of the seamount at 400 km indicated that it rose to a minimum depth of 3912 m just south of our track. The feature at 1530 km showing a marked depression on both sides of the raised central section belongs to the Mendocino Fracture Zone.

Thermal Structure of the Water and Sound Speed Profiles

Two types of Sippican XBT were employed -- a mod T7 having a design depth of 760 m and a mod T5 having a design depth of 1800 m. The intention was to sample the more stable deep layers less frequently than the unstable shallow layers by interspersing the more expensive mod T5 among the mod T7 XBT casts. The results are disappointing in that, although either the T5 or T7 casts taken as a group are consistent, the two groups are not consistent with one another. The T7 casts resemble the T5 casts down to about 400 m, but the T7 casts indicate a significantly lower temperature from 400 m to 760 m. Based on the facts that the T5 casts agree better with archival data [1] (the very low temperatures indicated by the T7 casts from 400 m to 760 m disagree with archival data) and that the pattern of explosive-shot arrivals was successfully modeled by using T5 profiles, the T7 casts have been set aside. The bathymetric measurements and the sound speed profiles derived from T5 XBT casts along the 1700-km radial track of this experiment are summarized in Fig. 4.

ACOUSTIC DATA

Figure 5 contains a representative sample of the heterodyned and digitized signal received from the 15-Hz source. The Hilbert transform of this digital signal was computed and used in conjunction with the navigation to obtain the signal amplitude at 0.5-km intervals. This spatial sampling rate exceeds the Nyquist rate. The amplitude is plotted in Fig. 6 as transmission loss vs range. Figures 7 and 8 are smoothed versions of Fig. 6 obtained by plotting the average received intensity over 7-km and 35-km intervals, respectively, as

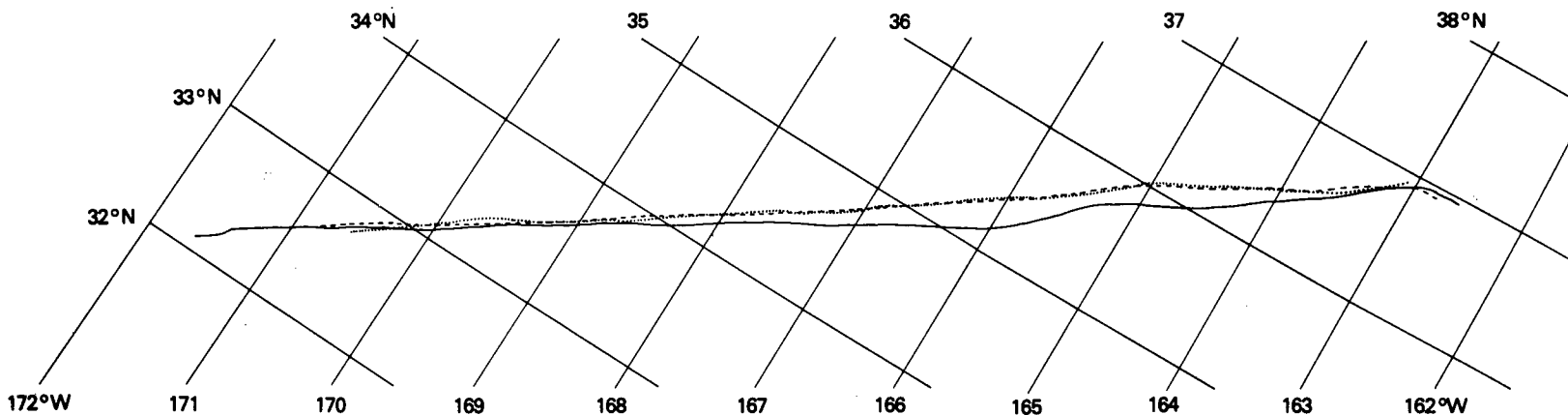


Fig. 2 — Gnomonic projection showing the details of the ship's track in phases two (solid), three (dashed), and four (dotted). Great circle tracks appear as straight lines in this projection.

CS

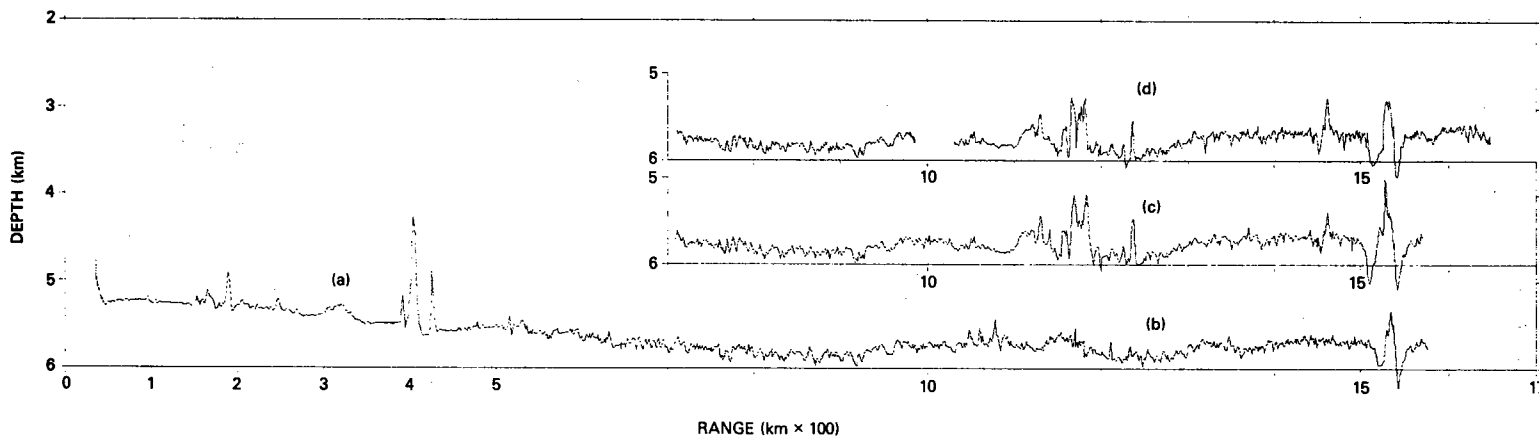


Fig. 3 — Measured bathymetry for an assumed sound speed of 1500 m/s in (a) phase one, (b) phase two, (c) phase three, and (d) phase four

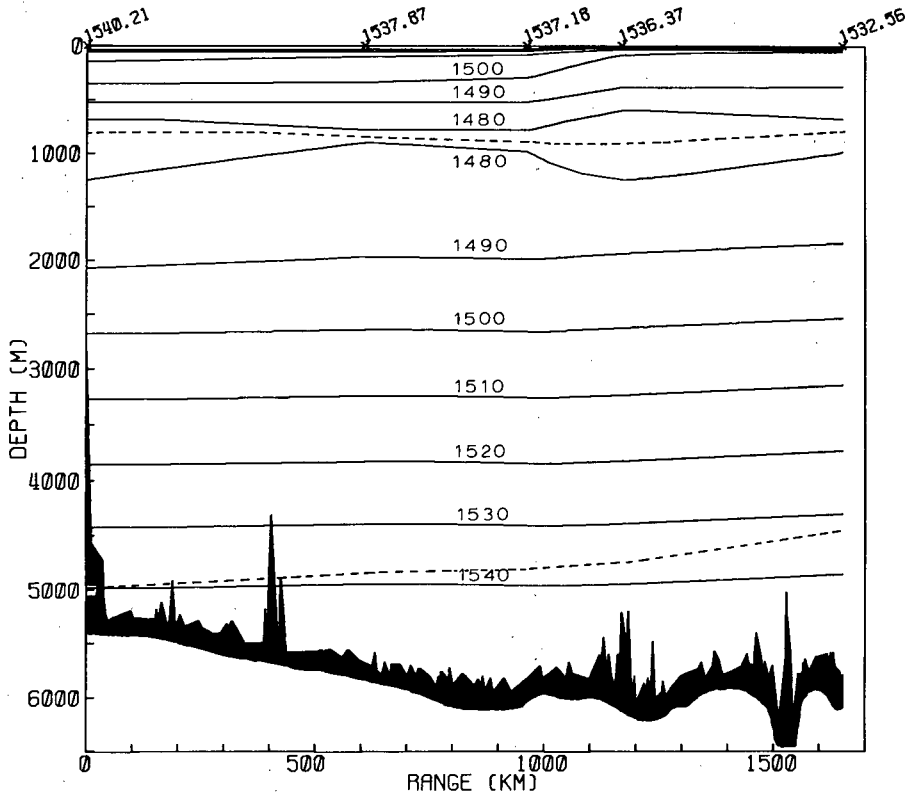


Fig. 4 — Environmental summary for phases one, two, three, and four. The SOFAR axis and critical depth are shown as dashed lines.

transmission loss vs range at the center of the interval. For the frequency, ranges, and nine-day time interval of the experiment, Fig. 8 gives an indication of the temporal stability of the mean transmission loss curve defined by a 35-km range average of intensity.

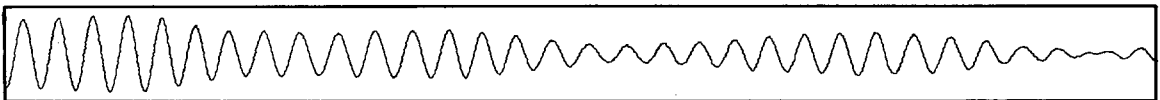


Fig. 5 — A typical 60-min sample of the digital acoustic data from the 15-Hz source in phase three. The digital signal was obtained by filtering and heterodyning the received signal and then sampling once every 2 s. The high signal-to-noise ratio is evident as is the stability of the phase and amplitude as the ship proceeds at 7 knots in the direction of the hydrophone.

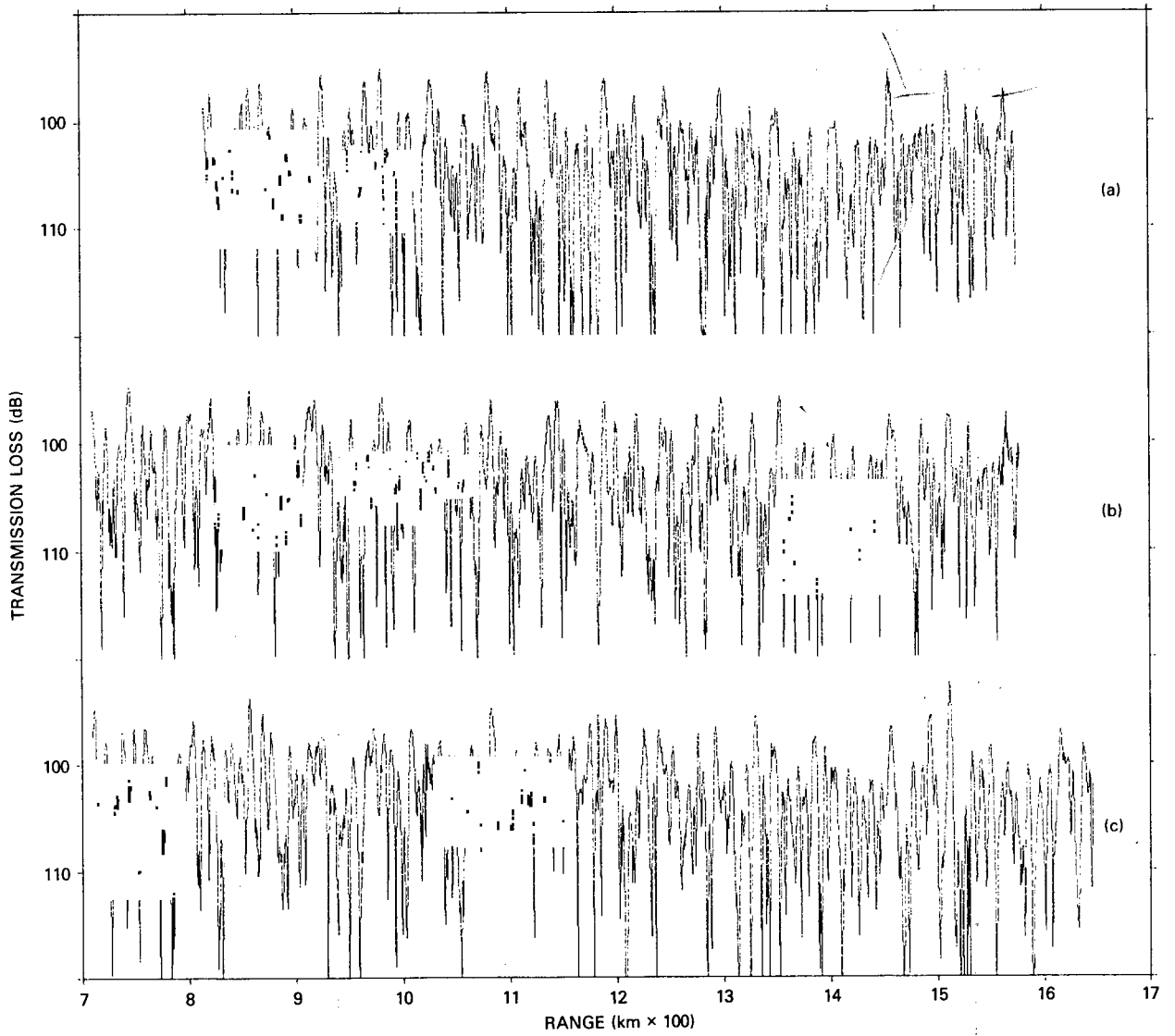


Fig. 6 — Transmission loss vs range of the 15-Hz signal for (a) phase two, (b) phase three, and (c) phase four. The spatial sampling rate is two samples/km.

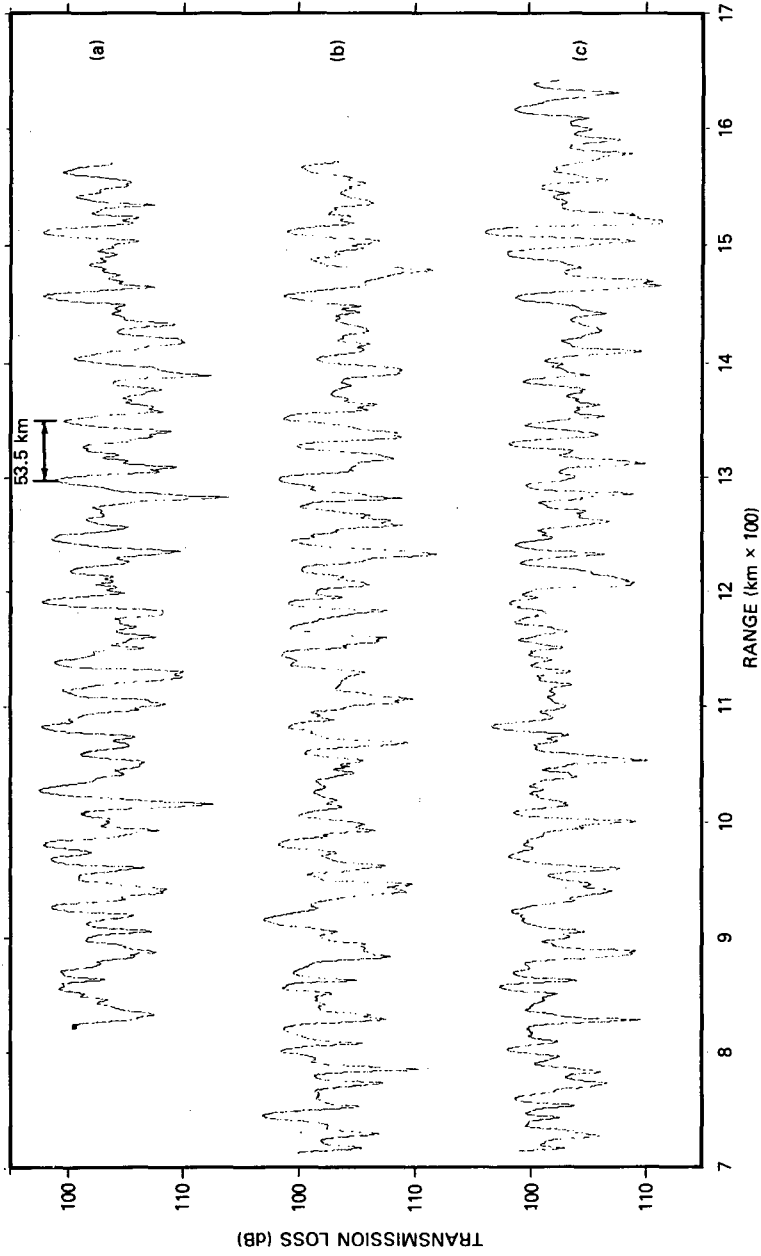


Fig. 7 — Transmission loss vs range (7-km running average of received intensity) of the 15-Hz signal for (a) phase two, (b) phase three, and (c) phase four

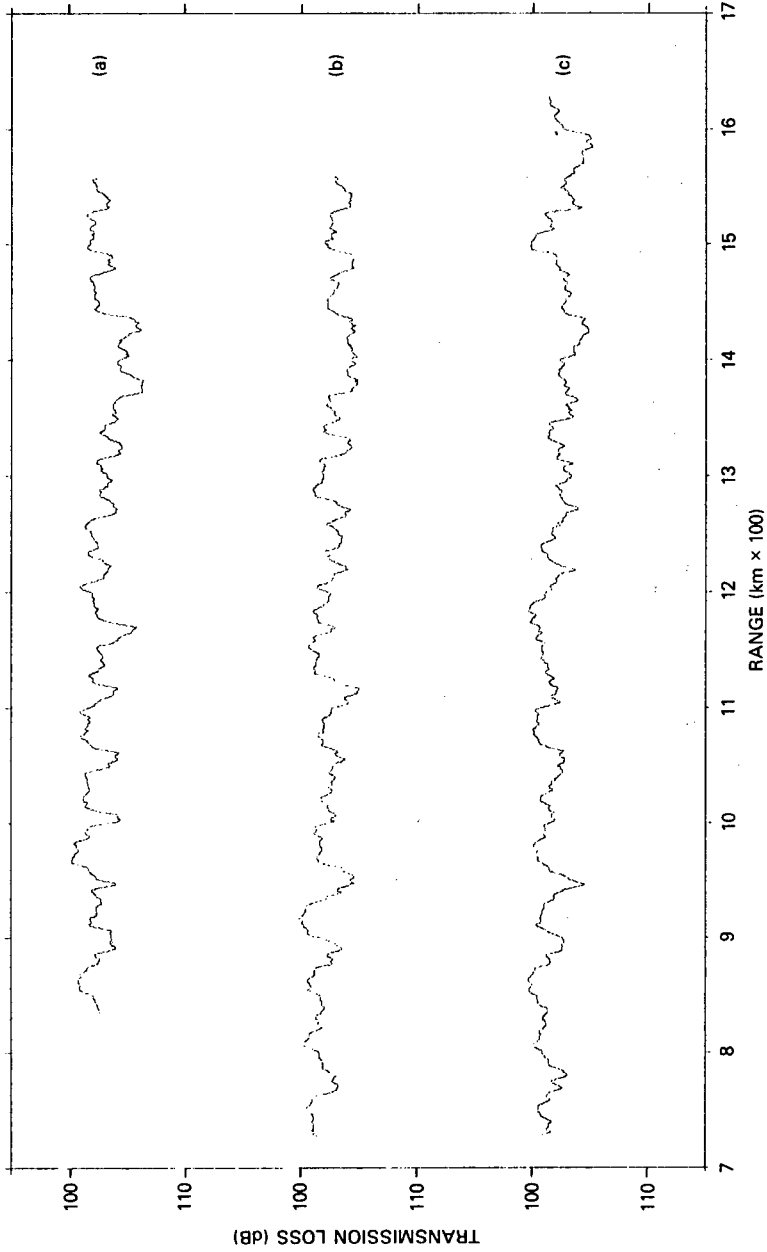


Fig. 8 — Transmission loss vs range (35-km running average of received intensity) of the 15-Hz signal for (a) phase two, (b) phase three, and (c) phase four

A noteworthy feature of Fig. 7 is the presence of zones of constructive interference at 53.5-km intervals with weaker such peaks appearing halfway between them. Figure 7(a) shows these features particularly well in the interval between 1000 km and 1600 km. The fact that the ship took 48 h to traverse this interval indicates a measure of long-term stability not only in the broad-area average transmission loss but also in some of the details of the interference pattern. The time interval from the beginning of phase two to the end of phase four includes nine full days; yet, some features of the interference pattern are repeated in all three phases.

In order to understand the observed periodicity, we employed a normal mode model of the acoustic field which required that the medium be specified by a single sound speed profile. Because Fig. 4 indicates a significant change in the ocean sound speed structure at a range of about 1000 km, two normal mode calculations were performed. The first calculation used the single sound speed profile of Fig. 9(a) which summarizes the water properties from 0- to 1000-km range. The second calculation used the profile of Fig. 9(b) which summarizes the water properties at ranges in excess of 1000 km. In both cases, the bottom was taken to be a flat, rigid reflector at a depth of 6000 m. The surface was modeled as a perfectly reflecting pressure release boundary, and no volume attenuation was considered. The neglected effect of volume absorption amounts to about 0.5 dB at 1000 km for 15 Hz [5]. To describe the modes and their properties we employ the ray-mode analogy and number the modes in the conventional manner so that mode 1 corresponds to the SOFAR axial ray. For both profiles, Fig. 9, (a) and (b), it is found that modes 1-19 correspond to RR rays, modes 20-27 correspond to RSR rays, and modes numbered greater than 27 correspond to BRSR rays.

A brief digression is in order at this point to consider the region of validity of this model. If the observed acoustic field depended strongly on the detailed acoustic properties and structure of the ocean bottom, the model's validity would be in grave doubt. As we shall see, the observed acoustic field is composed primarily of trapped modes which are relatively independent of the bottom properties. The higher order bottom-sensitive modes excited by the source are removed from the propagating acoustic field by their interaction with the ocean bottom. The normal mode calculation is valid in the sense that the calculated trapped modes model the experimentally observed field. Higher order bottom-sensitive modes are calculated in the model to demonstrate that if something more than just the trapped modes were present in the propagating field, the properties of the calculated field would disagree with those of the measured field. Simplicity and ease of calculation were the reasons for selecting the particular bottom model used to calculate higher order modes.

In the following paragraphs various comparisons are made between the experimental data and the calculated acoustic field. We consider first, the average received intensity over a 35-km range interval; second, the average received intensity over a 7-km range interval; and third, the spectrum of the range-dependent intensity corrected for cylindrical spreading.

Figure 10 shows a comparison between the 35-km average intensity of phase two (Fig. 8(a)) and the calculated average for the profile of Fig. 9(a). It is clear that the RR modes alone are capable of accounting for the average received intensity. If we consider the possible errors in source level and system response, however, this comparison between model and data is taken to be more suggestive than conclusive. Figure 11 shows a similar

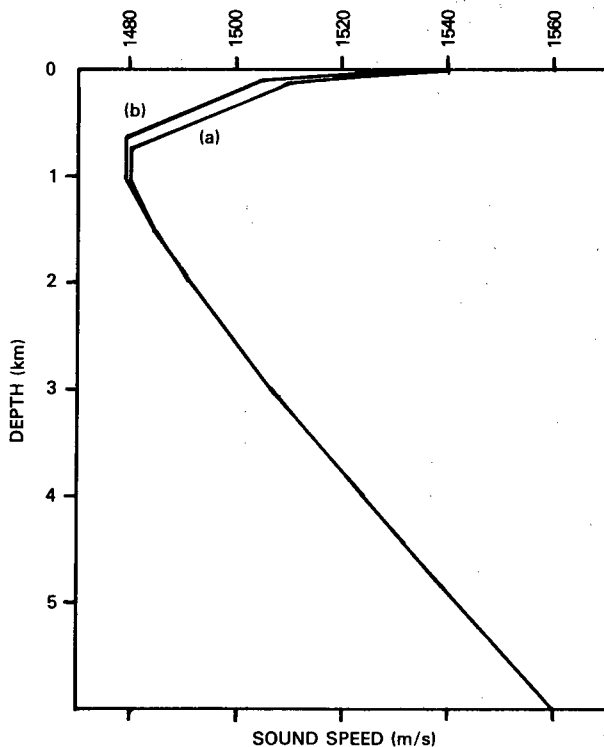


Fig. 9— Sound speed profiles used in the normal mode calculations. Profiles (a) and (b) characterize the environmental properties for ranges less than and greater than 1000 km, respectively.

comparison between the data and the calculated average intensity for the profile of Fig. 9(b). Again the RR modes are sufficient to explain the received intensity.

Figure 12 shows the average intensity received over a 7-km interval as calculated for the profiles of Fig. 9. In the range interval 1300 to 1700 km, Fig. 12 shows zones of constructive interference at 53.5-km intervals with secondary peaks midway between. The RR modes producing these peaks have deep turnaround points between 3000- and 3600-m depths. Such modes would propagate with little interference from the topography of Figs. 3 and 4. Although Fig. 12 is conditioned by such caveats as (i) only modes 1 to 12 were summed to obtain the pressure (which causes the calculated transmission loss to be higher than that of the experimental data) and (ii) the ranges of the calculated and experimental transmission loss peaks do not match, it is significant that the observed periodicity in the experimental transmission loss can be modeled by the same subset of RR modes for either profile in Fig. 9.

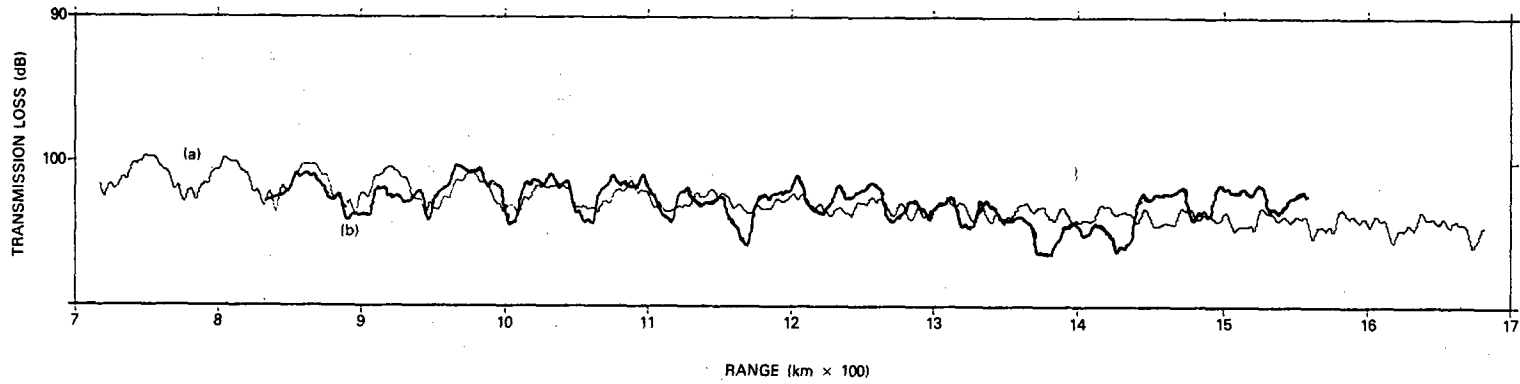


Fig. 10 — Comparison of measured and calculated average transmission loss. The thicker line shows the 35-km running average of received intensity for phase two plotted as transmission loss vs range (i.e. the thicker line is a duplicate of Fig. 8(a)). The thinner line shows a 35-km running average of received intensity calculated for the profile of Fig. 9(a). Only the first 19 modes, which correspond to the RR rays, were included in the mode summation.

10

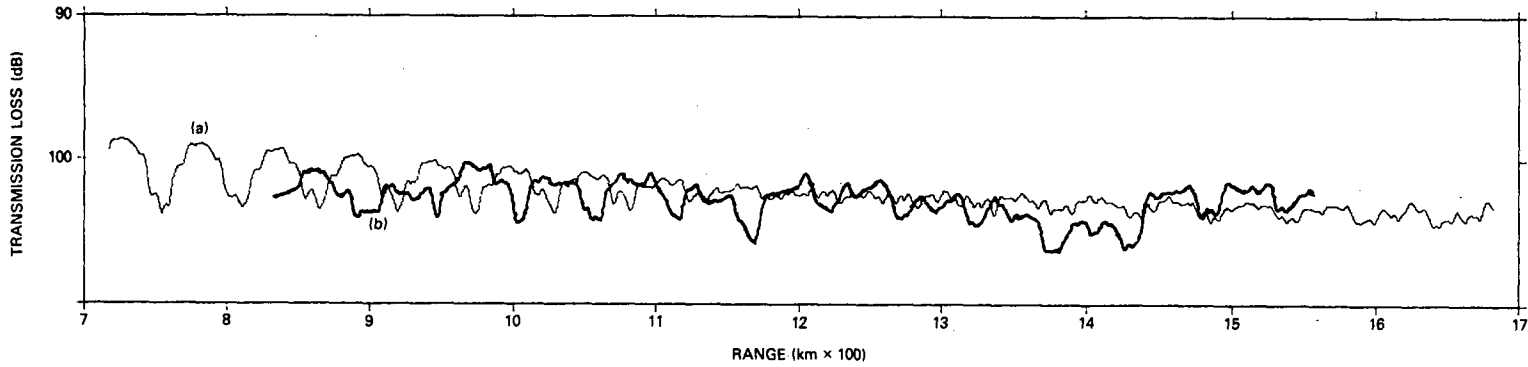


Fig. 11 — Comparison of measured and calculated average transmission loss. The thicker line shows the 35-km running average of received intensity for phase two plotted as transmission loss vs range (i.e. the thicker line is a duplicate of Fig. 8(a)). The thinner line shows a 35-km running average of received intensity calculated for the profile of Fig. 9(b). Only the first 19 modes, which correspond to RR rays, were included in the mode summation.

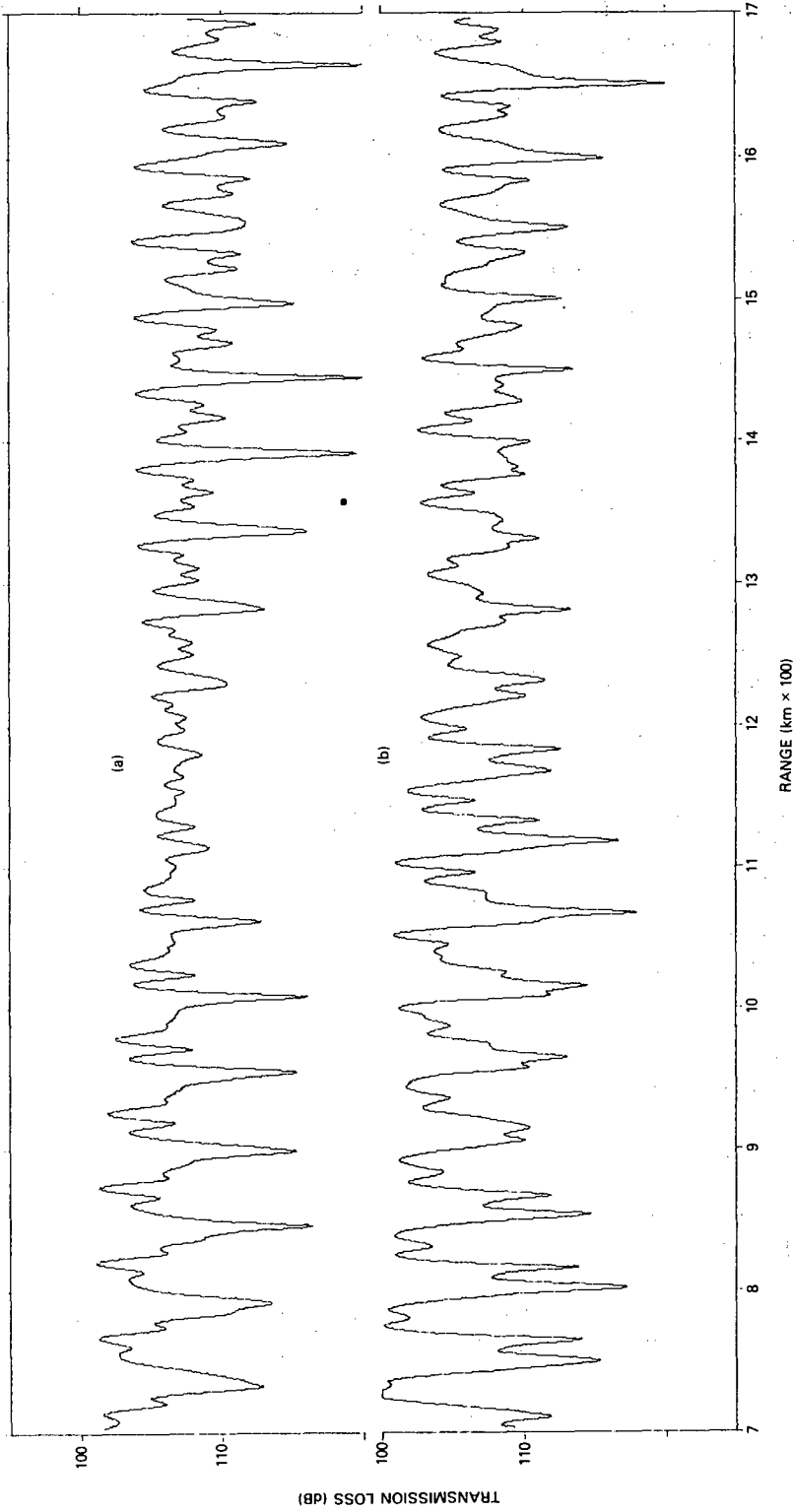


Fig. 12 — (a) The 7-km running average of received intensity plotted as transmission loss vs range for the first 12 RR modes of the profile in Fig. 9(a); (b) the 7-km running average of received intensity plotted as transmission loss vs range for the first 12 RR modes of the profile in Fig. 9(b). The transmission loss curves between 1300 km and 1700 km show the periodic structure observed in the data of Fig. 7.

The normal mode model of acoustic intensity, $\langle p^2 \rangle$, when only a finite number N of modes propagates between a source and receiver at fixed depths, is given by

$$\langle p^2 \rangle = r^{-1} \sum_{m,n=1}^N A_m A_n \cos(k_m - k_n)r, \quad (1)$$

where A_m describes the excitation of mode m and r is the range. The radial wave number k_m is a monotonically decreasing function of the mode number m . Spectrum analysis of $r\langle p^2 \rangle$ yields information regarding the distribution of components $k_m - k_n$ present in the data. The largest difference, $k_{max} - k_{min}$, corresponds to interference between the excited, propagating modes having the lowest and highest mode numbers. Thus another estimate of the number of propagating modes present in the data can be obtained by a comparison of the falloff in the data spectra of $\langle p^2 \rangle$ as $k_m - k_n$ increases with the falloffs in the spectra of $\langle p^2 \rangle$ calculated for the profiles of Fig. 9 for various numbers of propagating modes.

Figure 13 shows spectra of $r\langle p^2 \rangle$ for intervals of 512 km beginning at the minimum range in each phase. Figures 14-17 show calculated spectra of $r\langle p^2 \rangle$ for the profile of Fig. 9(a). These spectra were obtained from the calculated values of $\langle p^2 \rangle$ at 0.5-km intervals from 700- to (700 + 512)-km ranges. All spectrum levels are given in decibels relative to the same arbitrary level. If we compare Fig. 13 with Figs. 14-17, it appears that the highest mode number of a propagating mode is about 19. Again the conclusion is that no bottom-interacting modes appear in the experimental spectrum.

This type of analysis is insensitive to errors in source level and system response, provided that the errors do not change with time. During the course of the experiment and in the processing of the data, no changes were made in the responses of the low-frequency receiving and processing systems. The 15-Hz source level could not vary, because the source has fixed-displacement pistons. The spectrum analysis is conservative in determining an upper bound on propagating mode number in that it assumes temporal stability in the transmission loss curve over the approximately 40 h required for the ship to go 512 km. Temporal variations in transmission loss with periods of 10 min or less (corresponding to range intervals of 2 km or less for a ship at 7 knots) would appear in the data spectrum indistinguishable from contributions of BRSR modes. In addition, the spectrum analysis is conservative in estimating an upper bound on propagating mode number, because we have compared the data spectra with spectra calculated by using a normal mode model in a range-independent medium. Any range dependence present in the ocean, whether in the sound speed profile or in the bathymetry (cf. Fig. 4), produces coupling among the modes which form a mathematical basis for the acoustic field. Such an increase in the number of basis functions would appear in the spectra indistinguishable from contributions of higher order propagating BRSR paths.

Similar conclusions can be drawn from Fig. 13 by comparing it with an even simpler model of the acoustic field. Suppose there are N propagating modes with

$$A_m = 1 \quad (2)$$

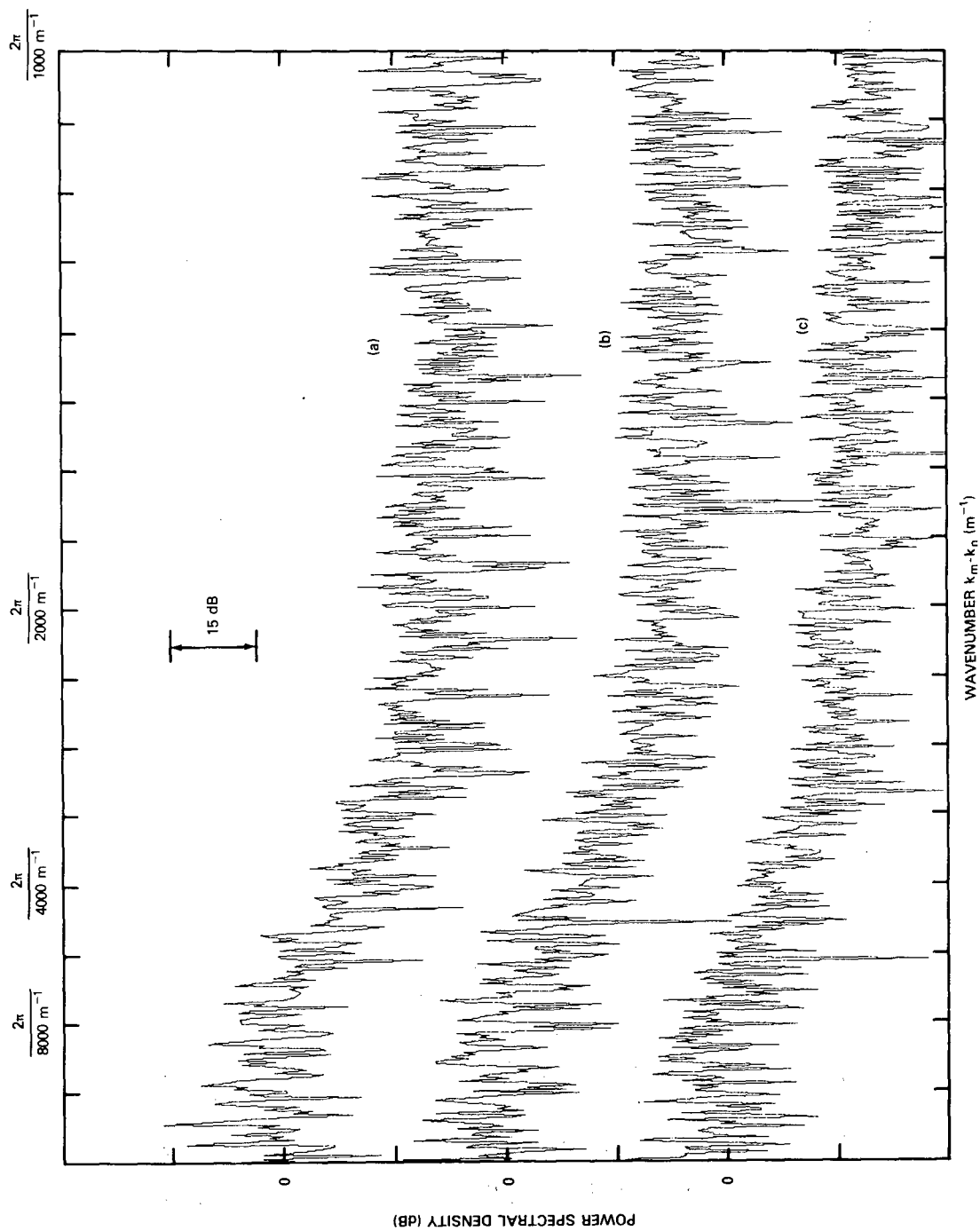


Fig. 13 — Power spectral density of $r \langle p^2 \rangle$ for the first 512 km of (a) phase two, (b) phase three, and (c) phase four

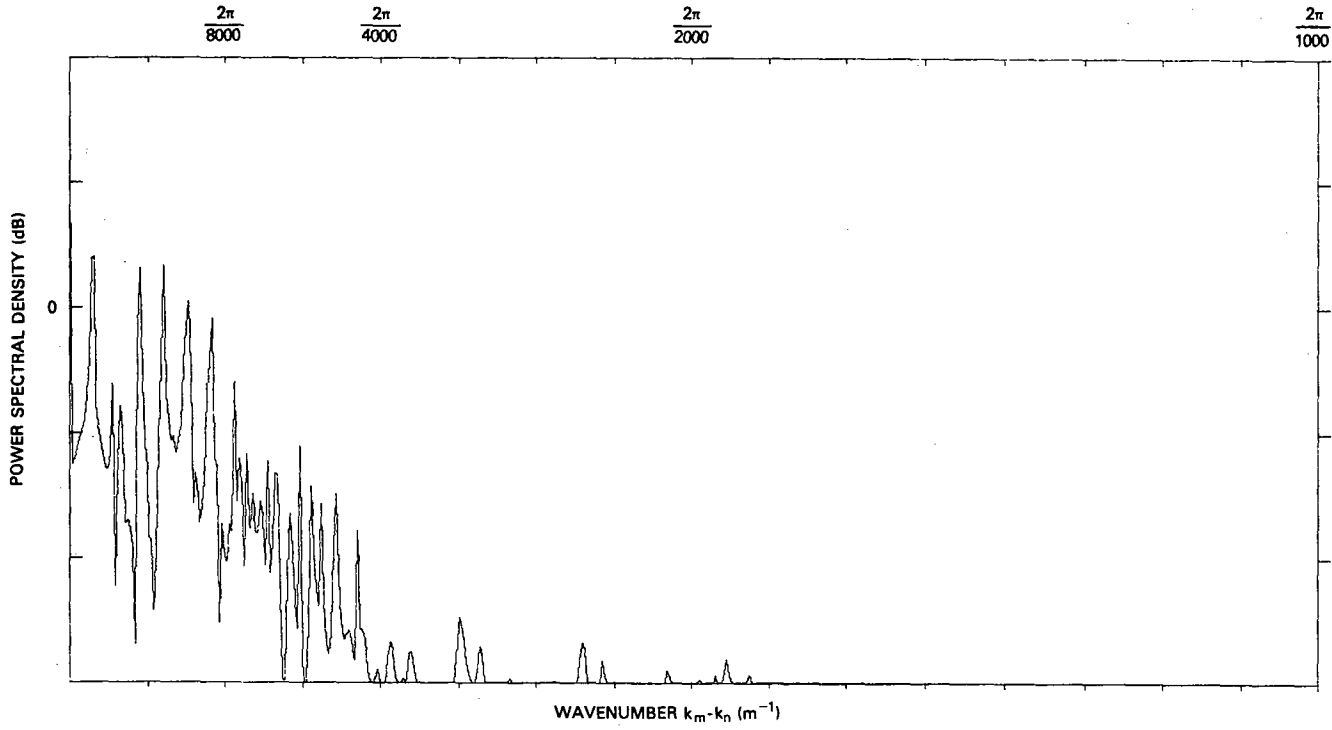


Fig. 14 — Power spectral density of $r\langle p^2 \rangle$ for ranges 700 to $(700 + 512)$ km and for the first 12 modes of the profile of Fig. 9(a). The appearance of spectral components to the right of $k_m - k_n = 2\pi/2307 m^{-1}$ in this figure is due to leakage associated with the use of a rectangular data window and to finite computer word size.

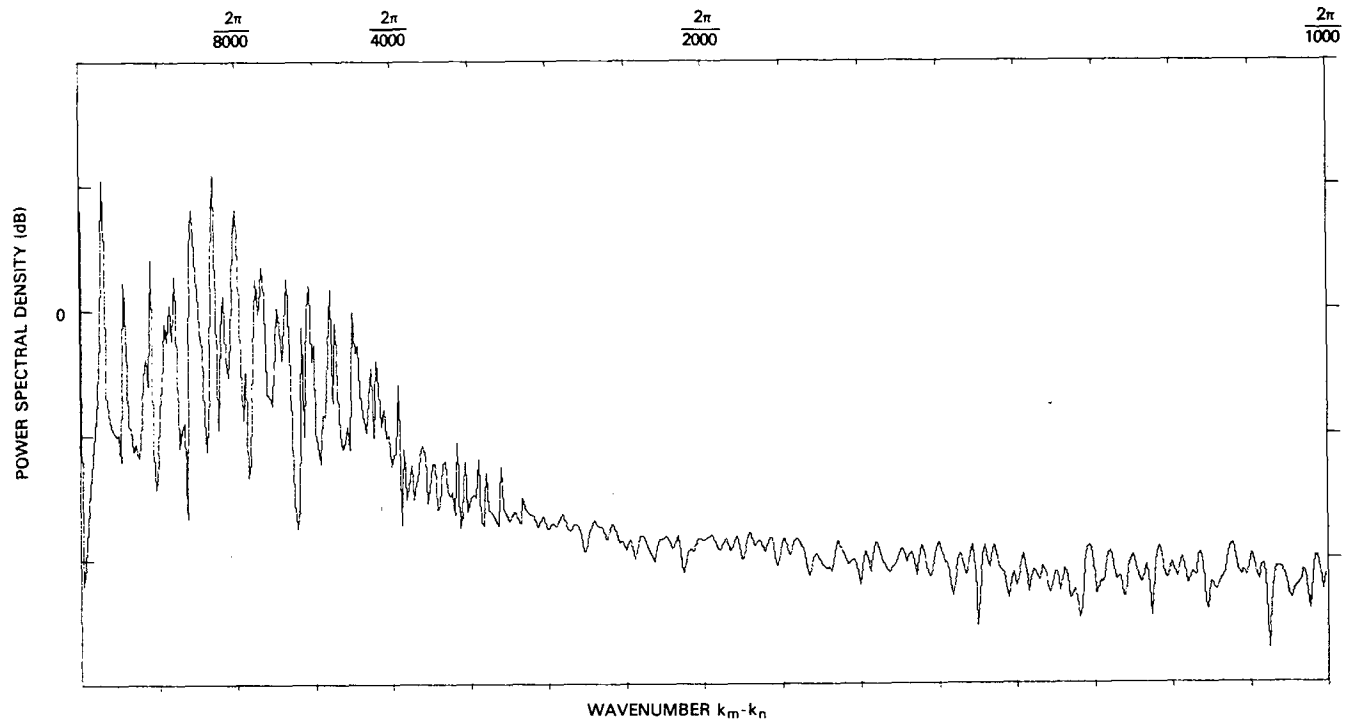


Fig. 15 — Power spectral density of $r\langle p^2 \rangle$ for ranges 700 to $(700 + 512)$ km and for the first 19 modes of the profile of Fig. 9(a). The appearance of spectral components to the right of $k_m - k_n = 2\pi/2819 \text{ m}^{-1}$ in this figure is due to leakage associated with the use of a rectangular data window and to finite computer word size.

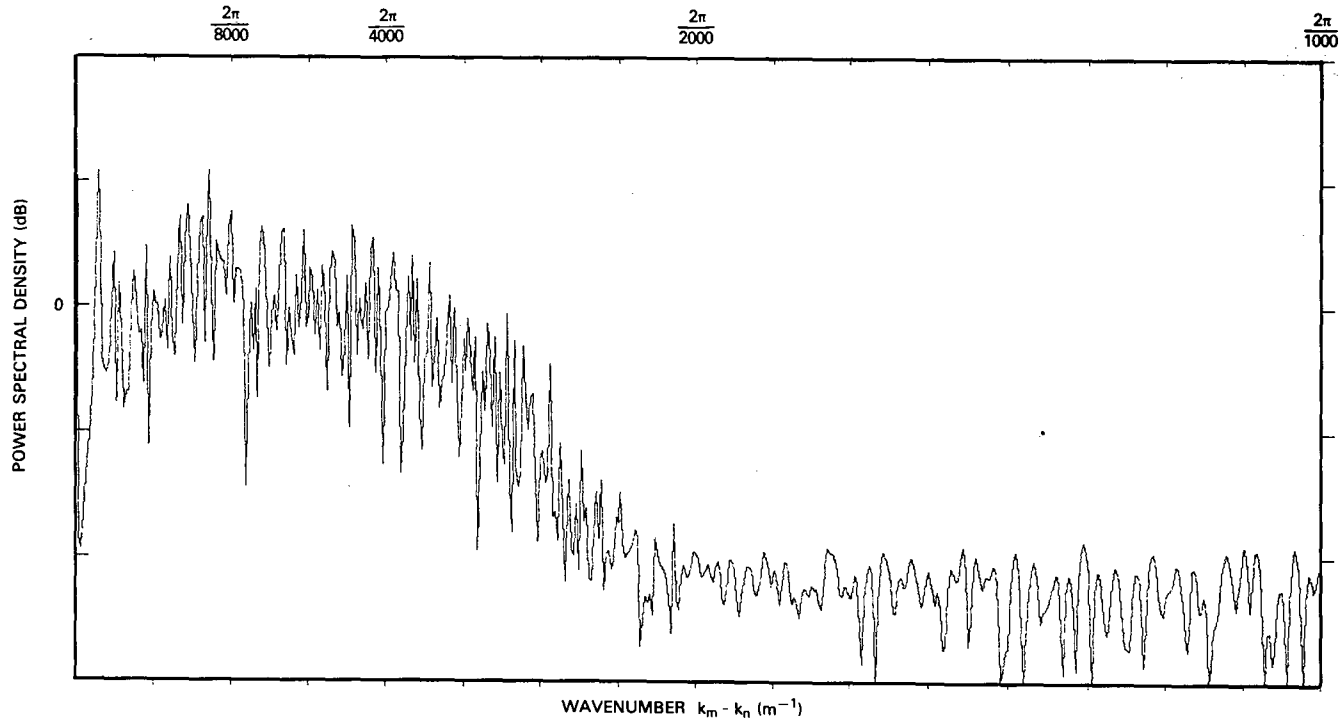


Fig. 16 — Power spectral density of $r\langle p^2 \rangle$ for ranges 700 to $(700 + 512)$ km and for the first 27 modes of the profile of Fig. 9(a). The appearance of spectral components to the right of $k_m - k_n = 2\pi/2076 \text{ m}^{-1}$ in this figure is due to leakage associated with the use of a rectangular data window and to finite computer word size.

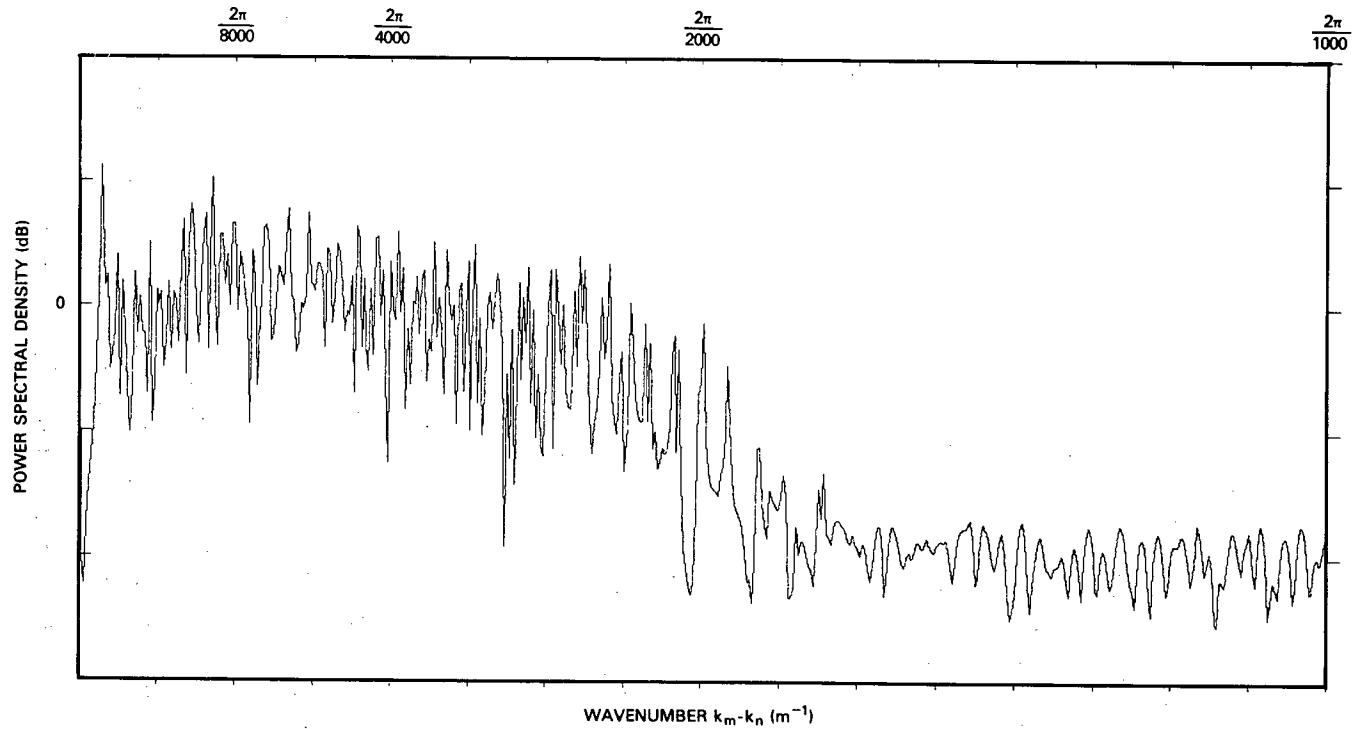


Fig. 17 — Power spectral density of $r\langle p^2 \rangle$ for ranges 700 to $(700 + 512)$ km and for the first 34 modes of the profile of Fig. 9(a). The appearance of spectral components to the right of $k_m - k_n = 2\pi/1610 \text{ m}^{-1}$ in this figure is due to leakage associated with the use of a rectangular data window and to finite computer word size.

and

$$k_m = k + ma \quad (3)$$

for

$$m = 1, 2, \dots, N, \quad (4)$$

where k and a are constants. Equation (1) becomes

$$\begin{aligned} r\langle p^2 \rangle &= \sum_{m,n=1}^N \cos(m-n) a r \\ &= N + 2(N-1) \cos a r + 2(N-2) \cos 2 a r + \dots + 2 \cos(N-1) a r, \end{aligned} \quad (5)$$

which is in the form of a Fourier series. If we neglect the dc peak, the average power spectrum of $r\langle p^2 \rangle$ will fall off by 15 dB when

$$15 \simeq 20 \log \frac{2(N-1)}{2(N-j)} \quad (6)$$

or when

$$\frac{j}{N} \simeq 1 - 10^{-15/20} (1 - N^{-1}) \quad (7)$$

If we assume, conservatively, that

$$N \geq 5, \quad (8)$$

then Eq. (7) implies

$$j/N \geq 0.86 \quad (9)$$

at the point in the spectrum where the average is down by 15 dB.

From Fig. 13 it appears that the power spectrum of $r\langle p^2 \rangle$ is down 15 dB certainly by

$$k_m - k_n = \frac{2\pi}{4000} m^{-1}. \quad (10)$$

If $2\pi/4000 m^{-1}$ is 86% of the value of $k_{max} - k_{min}$, which corresponds to the interference between the lowest and highest numbered propagating modes, then

$$k_{max} - k_{min} = 2\pi/(4000 \times 0.86). \quad (11)$$

The lowest numbered, excited, propagating mode is reasonably approximated (and the approximation has been validated by the normal mode calculations) as the mode corresponding to the ray which turns over at the source depth, 142 m. The average speed of sound at the source depth was about 1502 m/s. This gives an estimate of the largest wave number as

$$k_{max} = \omega/1502 \text{ m}^{-1}. \quad (12)$$

Solving Eq. (11) for k_{min} and using Eq. (12) gives

$$k_{min} = \omega/1502 - 2\pi/(4000 \times 0.86). \quad (13)$$

The ray corresponding to this mode turns around at depths where the sound speed is given by

$$\begin{aligned} c &= \omega/k_{min} \\ &\approx 1548 \text{ m/s} \end{aligned}$$

for our source frequency. For the sound speed profiles of Fig. 4, this corresponds to an RSR ray which turns under at a depth of about 5400 m. Figure 4 shows that the bottom depth exceeds 5400 m over most of the track. This simple analysis again indicates the absence of propagating bottom-interacting paths.

ACKNOWLEDGMENTS

This work was supported by the Naval Electronics System Command. The data was obtained through the cooperation of the Commander, Pacific Missile Range. The authors wish to thank Seymour Adler, who served as senior scientist on board, and acknowledge the assistance of the officers and crew of the USNS *Gibbs* (T-AGOR-1). Ms. Marilyn L. Blodgett contributed significantly to the reduction of the acoustic data here reported.

REFERENCES

1. A.N. Guthrie, J.D. Shaffer, D.A. Nutile, and R.M. Fitzgerald, "Long-Range Propagation Experiment: Procedures and Shipboard Data," NRL Memo. Rept. 3405, November 1976.
2. D.A. Nutile and A.N. Guthrie, "Propagation Paths to Midway Island," J. Acoust. Soc. Am. 65, 70-74 (1979).
3. D.A. Nutile and A.N. Guthrie, "Acoustic Shadowing by Seamounts," submitted to J. Acoust. Soc. Am.
4. R.M. Fitzgerald, A.N. Guthrie, and J.D. Shaffer, "Transverse Coherence of Low-Frequency Acoustic Signals," NRL Report 8241, August 1978.
5. W.H. Thorp, "Deep-Ocean Sound Attenuation in the Sub- and Low-Kilocycle-per-Second Region," J. Acoust. Soc. Am. 38, 648-654 (1965).